REPORT DOCUMENTATION PAGE

Form Approved
OMB No. 0704-0188

1. REPORT DATE	2. REPORT TYPE	3. DATES COVERED
	Professional Paper	

4. TITLE AND SUBTITLE

Experimental and Numerical Investigation of Vortex Shedding of a Representative UCAV Configuration for Vortex Flow Control

5a. CONTRACT NUMBER

5b. GRANT NUMBER

5c. PROGRAM ELEMENT NUMBER

6. AUTHOR(S)

Terence A. Ghee
Doug R. Hall

5d. PROJECT NUMBER

5e. TASK NUMBER

5f. WORK UNIT NUMBER

7. PERFORMING ORGANIZATION NAME(S) AND ADDRESS(ES)

Naval Air Warfare Center Aircraft Division
22347 Cedar Point Road, Unit #6
Patuxent River, Maryland 20670-1161

8. PERFORMING ORGANIZATION REPORT NUMBER

9. SPONSORING/MONITORING AGENCY NAME(S) AND ADDRESS(ES)

10. SPONSOR/MONITOR'S ACRONYM(S)

11. SPONSOR/MONITOR'S REPORT NUMBER(S)

12. DISTRIBUTION/AVAILABILITY STATEMENT

Approved for public release; distribution is unlimited.

13. SUPPLEMENTARY NOTES

14. ABSTRACT

15. SUBJECT TERMS

16. SECURITY CLASSIFICATION OF:			17. LIMITATION OF ABSTRACT	18. NUMBER OF PAGES	19a. NAME OF RESPONSIBLE PERSON
a. REPORT	b. ABSTRACT	c. THIS PAGE			Terence Ghee / Doug Hall
Unclassified	Unclassified	Unclassified	SAR	25	19b. TELEPHONE NUMBER (include area code) (301) 342-8536 / 342-8534

Standard Form 298 (Rev. 8-98)
Prescribed by ANSI Std. Z39-18

Experimental and Numerical Investigation of Vortex Shedding of a Representative UCAV Configuration for Vortex Flow Control

Terence A. Ghee *, Doug R. Hall †
NAVAIR, Code 4321
Bldg. 2187, Suite 1320B
Patuxent River, MD 20670-1906

INTRODUCTION

On vehicles with swept wings, leading edge vortices are created at off-design conditions, Ref. 1. The leading edge vortex generally has a beneficial effect in the form of increased lift. By controlling the location of the shed vortex or vortices, vehicle roll and pitch control may be possible. Uninhabited Combat Air Vehicles (UCAV) that utilize stealth to avoid detection suffer a radar signature increase when control surfaces are deflected. Thus, there is an advantage to be gained by limiting flap deflection by utilizing vortex flow control to change vehicle attitude. In view of this, an experimental and numerical investigation was conducted on a representative UCAV configuration to define the flowfield and investigate methods to control vortex location, and ultimately, vehicle attitude. In view of this, a test program was carried out to identify the flow features of a representative UCAV configuration and utilize a simple blowing jet near the nose of the vehicle to attempt vortex flow control.

EXPERIMENTAL SETUP

The tests were conducted in the Naval Aerodynamic Test Facility (NATF); a 4-foot by 4-foot closed test section, open return subsonic wind tunnel. Data were collected at tunnel velocities of 50 ft/s to 200 ft/s (M=0.04 to 0.18) while angle-of-attack was varied from 0 to 18 degrees in increments of 1 degree. However, for vortex manipulation effects, off-body flow surveys, and CFD comparison, a moderate angle-of-attack of 12 degrees was chosen.

A 4% UCAV model with 47-degree leading edge was used as a representative configuration, see Fig. 1. The model was fabricated of stainless steel by the US Air Force Research Laboratory and tested previously to assess aerodynamic performance, Ref. 2. The vehicle is a delta wing of a span of 2.16 feet, a reference wing area of 1.210 ft^2, and a mean aerodynamic chord of 0.765 feet. The normal nose engine inlet was eliminated through the use of a faired nose/propulsion inlet plug. The leading edge of the vehicle has a sharp chine at the nose that transitions to round in the vicinity of the wing/body juncture, see Fig. 2. Also visible in Fig. 2 are the transducers installed on the model. The nose/propulsion inlet plug allowed the testing of a more simplified geometry with out the added complexity of evaluating the flowfield that included a flow-through duct. In addition, transducer signal/power cables could be run through the flow-through duct and avoiding expensive machining of the model. The nose/propulsion inlet plug also allows the testing of novel vortex flow control devices, affixed to the plug, to be easily fabricated and evaluated.

TEST CONDITIONS AND SAMPLE RESULTS

The testing was conducted as part of the Naval Air Warfare Center In-House Laboratory Independent Research (ILIR) program and developed in three phases: 1) vortex location

* Aerospace Engineer, ph: 301 342 8536 FAX: 301 342 8588, gheeta@navair.navy.mil, Senior Member, AIAA
† Aerospace Engineer, ph: 301 342 8534, FAX: 301 342 8588, halldr@navair.navy.mil, Senior Member, AIAA

identification using laser light sheet flow visualization, 2) vortex quantification through surface and 3) off-body measurements, and vortex manipulation utilizing a simple blowing jet. This paper primarily reports the results of the first two phases of the program.

In the first phase, a flow visualization study was conducted utilizing laser light sheet and injected vaporized propylene glycol to seed the flow. A miniature camera was mounted to the support system sting and orthogonal to the light sheet. To quantify the location of the vortices in space, video data was acquired and a grid was placed in the plane of the light sheet. Using a known reference location on the grid, the vortex locations could be determined, Fig. 3 and 4. In addition, fluorescent oil flow visualization studies was conducted at an angle-of-attack of 10 degrees and for wind tunnel velocities of 75 ft/s, 100 ft/s, 125 ft/s, and 150 ft/s, see Fig. 5. The wing vortex was seen to emanate from the leading edge at an approximate location of x/l=0.167, y/b/2=0.184. A separate vortex was seen to originate at the nose of the vehicle. Computational fluid dynamics (CFD) analyses were used to predict the flowfield with good agreement in the basic flow structure, see Fig.6.

The CFD calculations were performed using the COBALT code, a time-accurate, unstructured Navier-Stokes model, see Ref. 4. The time step was 1/10,000 second, the grid model utilized a symmetry plane for the model, and employed a grid of 381,000 cells, see Fig. 7. However, only every eighth data point was reported in the final data. The calculation was subject to 1000 iterations and found to be fully converged after 500 iterations. Thus, the data presented is 500 data points over an individual time period of 0.0008 seconds.

From both CFD and experiment, two distinct vortex systems were found: one vortex emanating from the nose of the vehicle and a second vortex issuing from the wing leading edge. The wing vortex was thought to emanate at the transition from a sharp to rounded leading edge.

Following gross flow field identification, 13 Kulite fast-response pressure transducers were installed on the model to determine surface pressure and vortex shedding frequency. These transducers were installed at locations, shown in Fig. 8, to best capture the effect of the vortex over the wing upper surface. Unsteady pressure data was acquired for 30 seconds at a sample rate of 10,240 samples/second. The data was analyzed in the time domain and the frequency domain and compared with the results of a time-accurate CFD calculation, see Figs. 9 and 10. In the figures, the model is pitched to 10 degrees angle-of-attack with tunnel dynamic pressure set to approximately 26 psf. The coherent acoustic noise present in the freestream was removed from the data through the use of an unsteady static pressure probe. For this portion of the testing, a dummy balance was used to ensure as rigid a system as possible. Because the wind tunnel data was uncorrected for sting bending and downwash effects on angle-of-attack, the CFD calculations were determined at an angle-of-attack of 12 degrees. These experimental effects will be quantified when the model re-enters the wind tunnel for force and moment evaluation.

An uncertainty estimate of the data was undertaken to gage the accuracy of the test results. The unsteady pressure measurement accuracy was dictated by the quoted instrumentation repeatability of 0.1%. The effect of the accuracy of the A/D system and power supply was evaluated and found to be negligible on the data accuracy (however, these uncertainties were incorporated in the error analysis). The tunnel velocity varied in the test section by approximately 1% and fluctuated by approximately 0.75% at the tested tunnel velocity. Using a method outlined in Ref. 3, the

uncertainty in pressure coefficient was estimated to be 0.027. The highest and lowest resolvable frequencies were 4167 Hz and 0.03 Hz, respectively. These values were based on Nyquist criteria and dwell time. The frequency that could be resolved in the PSD was approximately 1Hz.

CFD calculations show a poor prediction of the pressure on the model, see Figs. 9a and 9b. This is most likely due to the lack of grid density in the vicinity of interest. Additional calculations are to include a refined grid in this region of the flow. A study was conducted to determine the effect of angle-of-attack was on the pressure coefficient data. For the range from 9 degrees to 12 degrees angle-of attack, the experimental pressure coefficient was seen to vary less than the difference between experimental and calculated data.

A Power Spectral Density (PSD) evaluation was conducted and the comparison with CFD prediction is shown in Fig. 10. The PSD evaluation was based on a method outlined in Ref. 5. The data were segmented into windows to allow thirty averages and corresponded to a frequency resolution of 1 Hz. No data overlapping was employed and a Hanning filter was used with a window length the same size as the data segments. The mean was eliminated from the PSD and coherence calculations and a 95% confidence criterion was used to gage the assessment. In general, CFD performs rather poorly in predicting the amplitude of the signal. The frequency content prediction approximates the experimental data, but is not stellar. Part of the reason for the failure of CFD to predict the experimental data is the limited amount of CFD data available. As reported previously, an artificially limited amount of data was recorded from the CFD prediction. This limited amount of data has been found to violate the Nyquist criteria for the higher significant frequencies found in the experimental data. The CFD predictions are currently being re-run to obtain all the data calculated and thus will have a sample rate of 10,000 samples/second.

In addition to the surface pressure measurements, off-body measurements of the flowfield was undertaken using a three-component hot wire system mounted on a traverse, see Fig.11. Data from this portion of the testing is currently being acquired at a tunnel dynamic pressure of approximately 26 psf (150 ft/s) and at an angle-of-attack of 10 degrees. Once again, the dummy balance was installed to reduce the support system/model vibration. The grid resolution of the data was 1/8 inch (or 0.0048 y/b).

The paper will present results from the present testing and show comparison to CFD prediction. Lessons learned and strengths and weakness of the CFD predictions will also be presented. Attention will be drawn to the fundamental flow features and underlying physics. Finally, an assessment of possible vortex control using nose jet blowing will be discussed.

References:

1. Kulfan, R.M., "Wing Airfoil Shape Effects on the Development of Leading Edge Vortices," AIAA Paper 79-1675, Reno, NV, January 1979.

2. Billman, G.M., Osborne, B.A., "High L/D Extended Range/Payload Fighter Aircraft Technology," AFRL-VA-WP-TR-1999-3084, November 1998.

3. Rae, W.H., Pope, A. Low-Speed Wind Tunnel Testing, 2nd Edition, Wiley, New York, 1984.

4. Strang, W.Z., "parallel Cobalt User's Manual," AFRL, CFD Research Branch Report, Wright-Patterson AFB, OH, September 1999.

5. Welch, D.G., "The Use of Fast Fourier Transform for the Estimation of Power Spectra: A Method Based on Time Averaging Over Short, Modified Periodograms," *IEEE Trans. Audio Electroacoust.*, Vol. AU-15, June 1967.

Fig. 1- UCAV in NATF

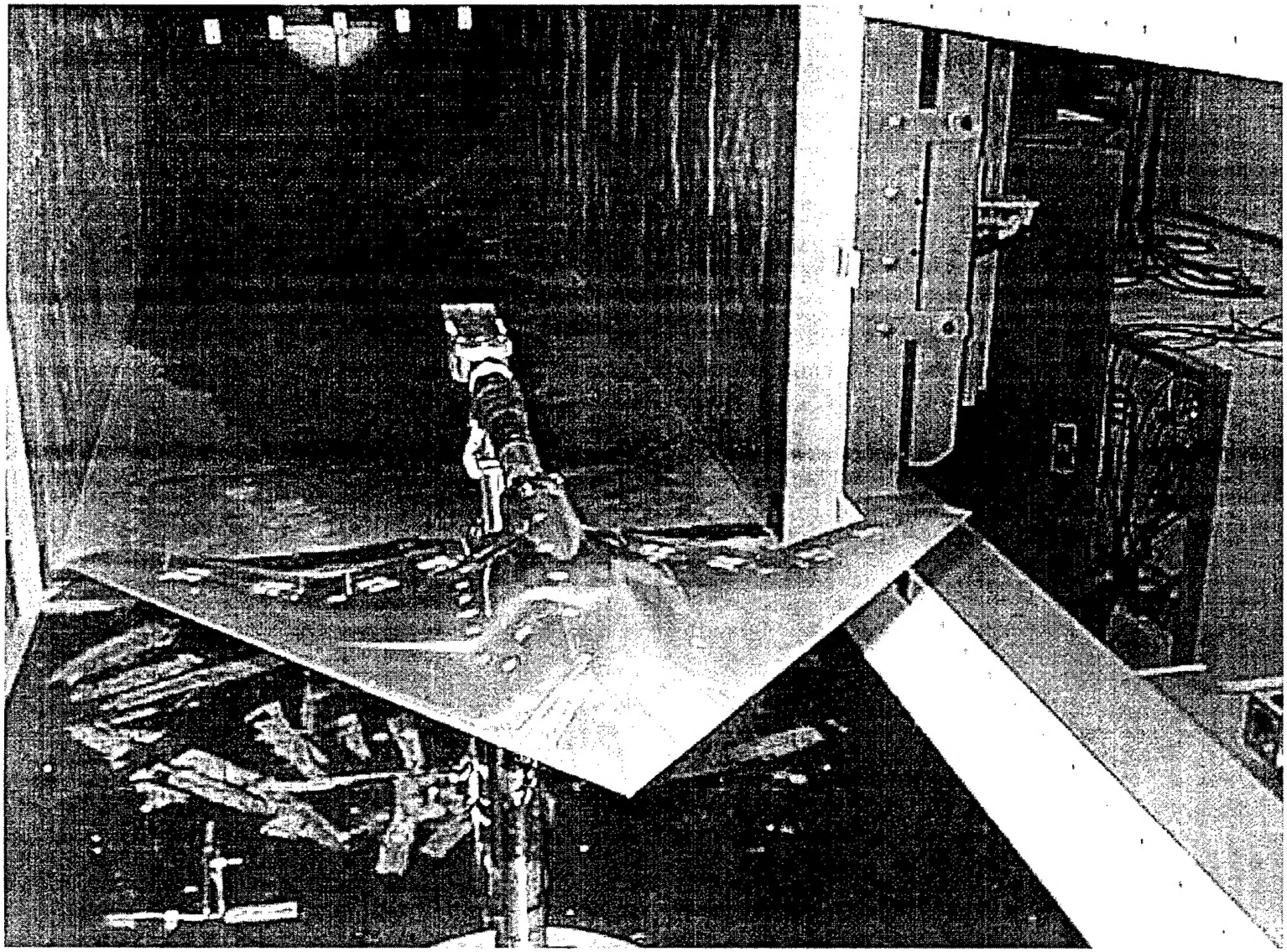

Fig. 2- UCAV Leading Edge

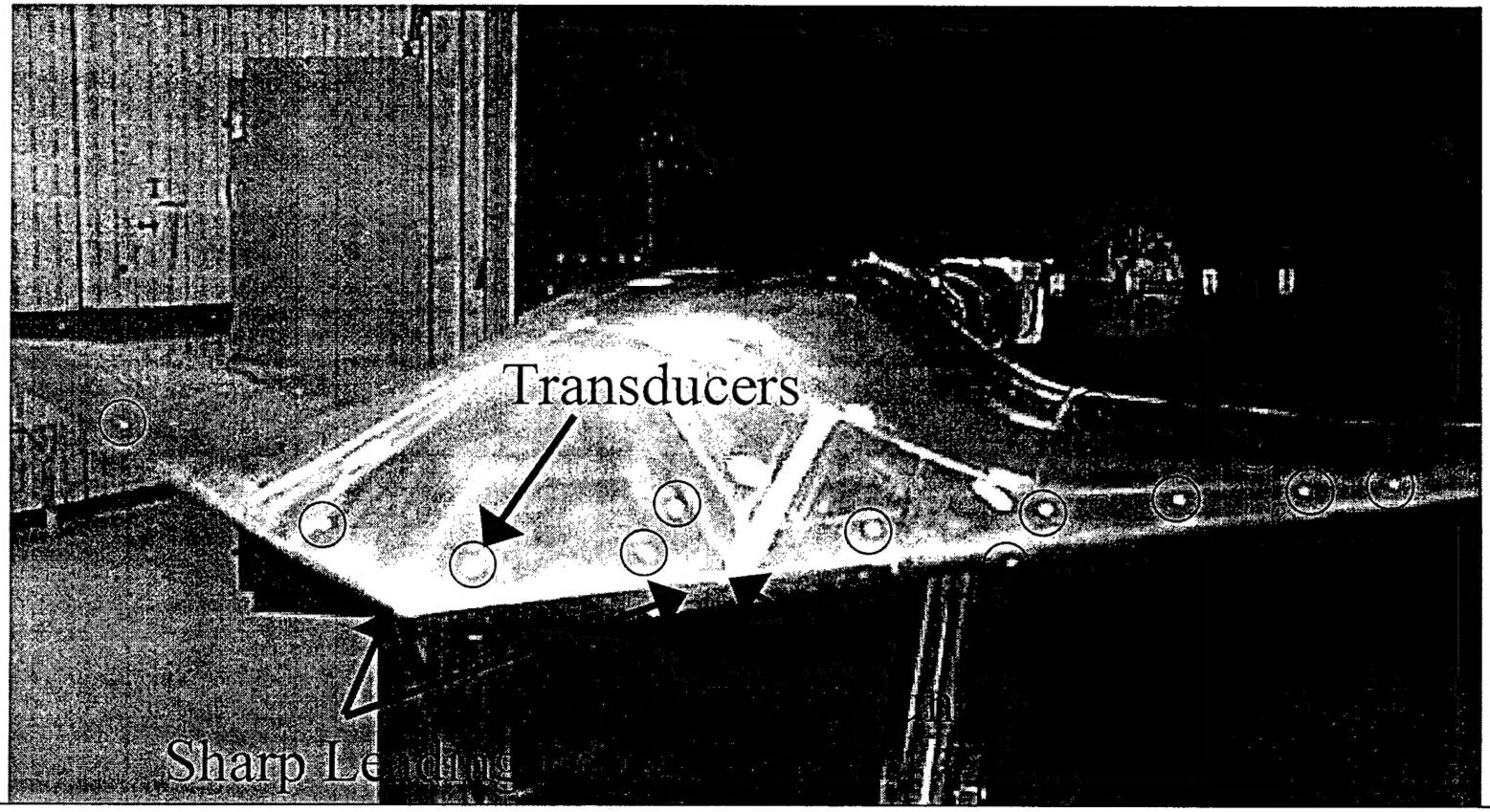

Fig. 3 - Vortex Location Using Laser Light Sheet: X/c=0.439

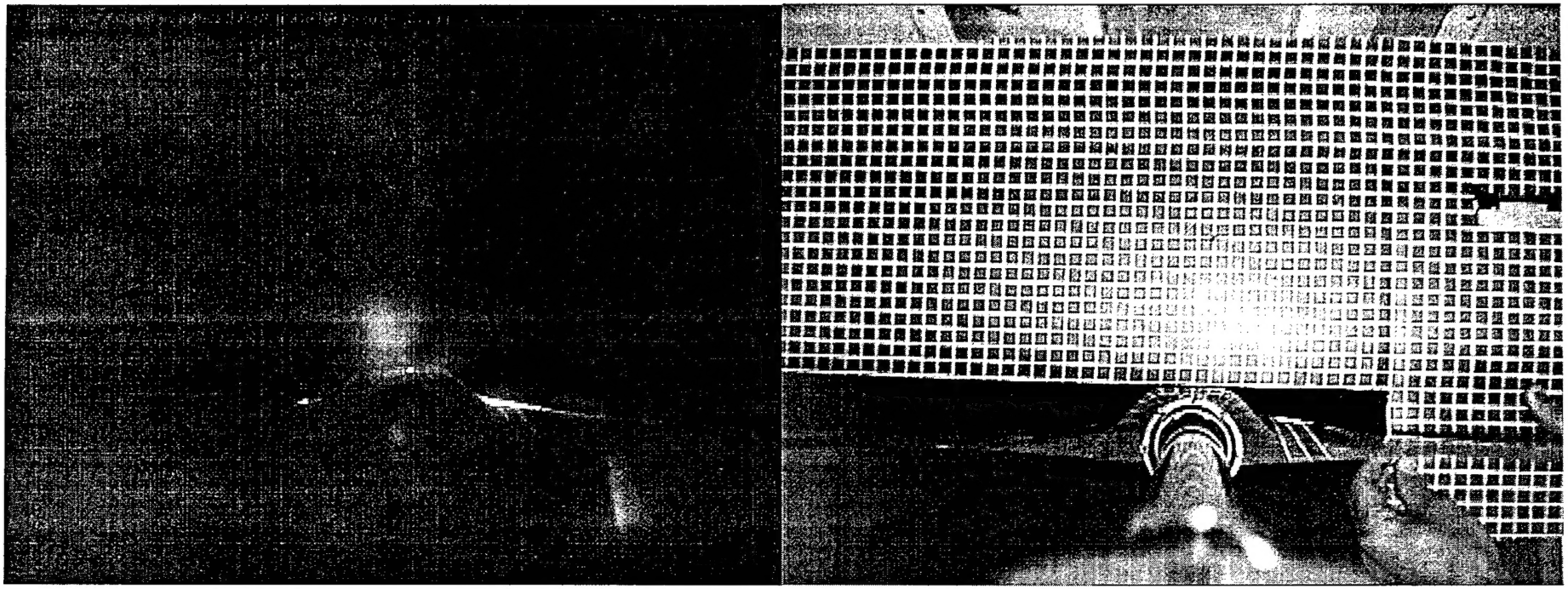

a) Video data, view looking upstream.

b) Reference grid video, used to quantify vortex location.

Fig. 4- Vortex location at 12 degrees angle-of-attack.

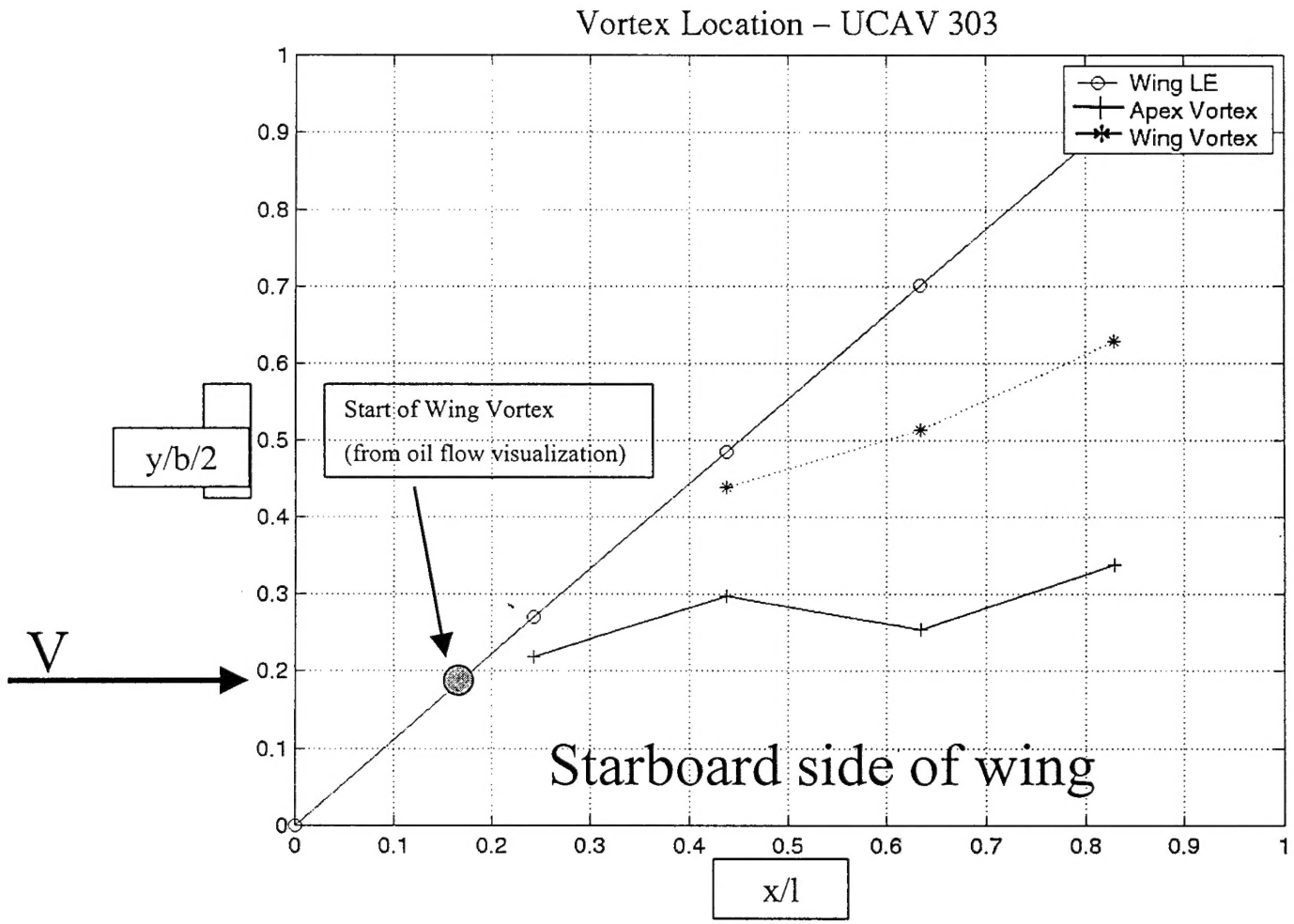

Fig. 5- Oil flow at 10 deg. AoA

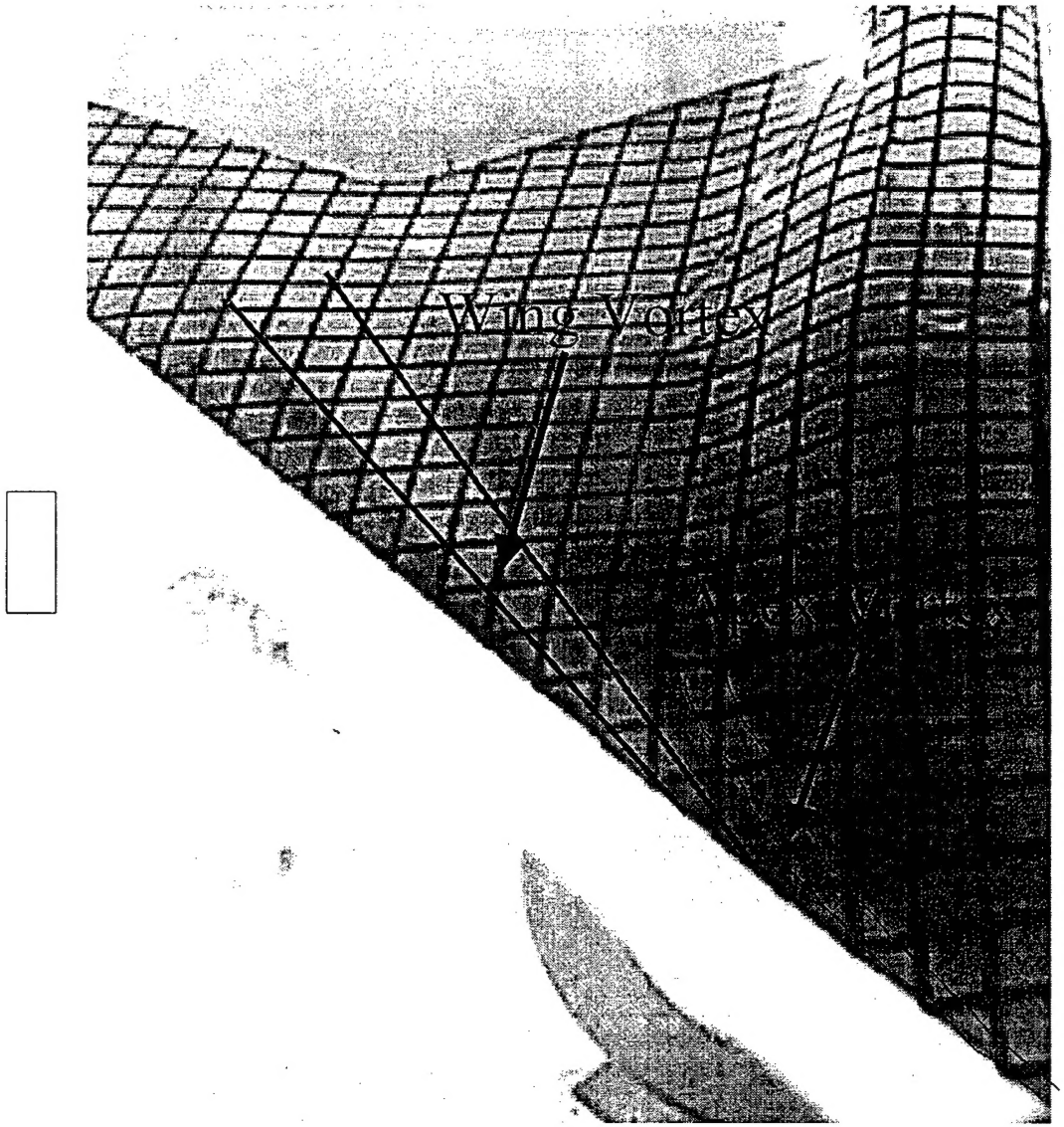

Fig. 6- CFD "flow visualization"

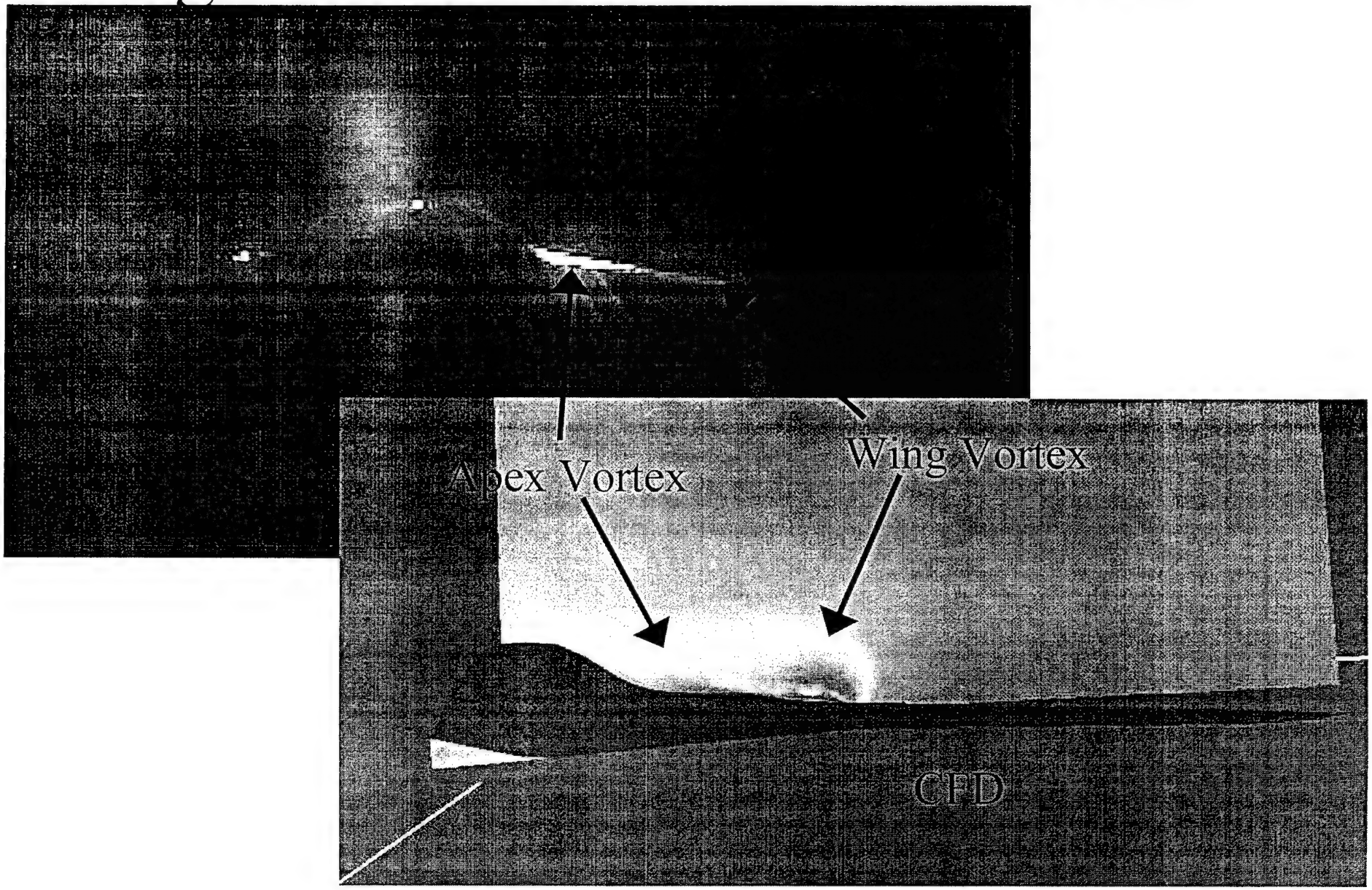

Fig. 7- CFD Grid

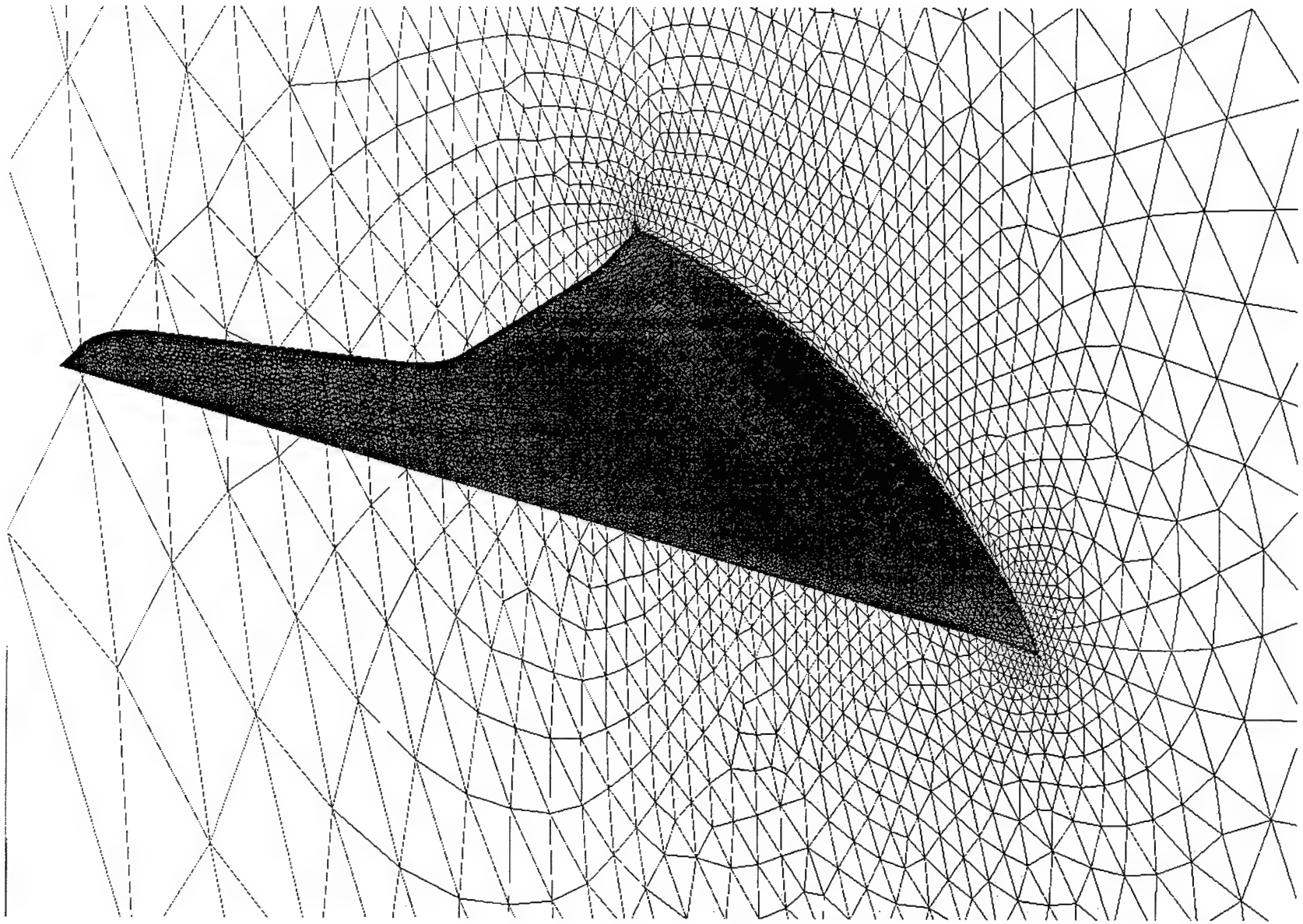

Fig. 8- Transducer location

#	X/c	Y/b
1	0.047	0.008
2	0.131	0.036
3	0.183	0.038
4	0.161	-0.044
5	0.263	0.078
6 (lower surf.)	0.352	0.108
7	0.377	0.116
8	0.476	0.148
9	0.581	0.183
10	0.665	0.211
11	0.609	-0.192
12	1.154	0.132
13	1.115	0.257

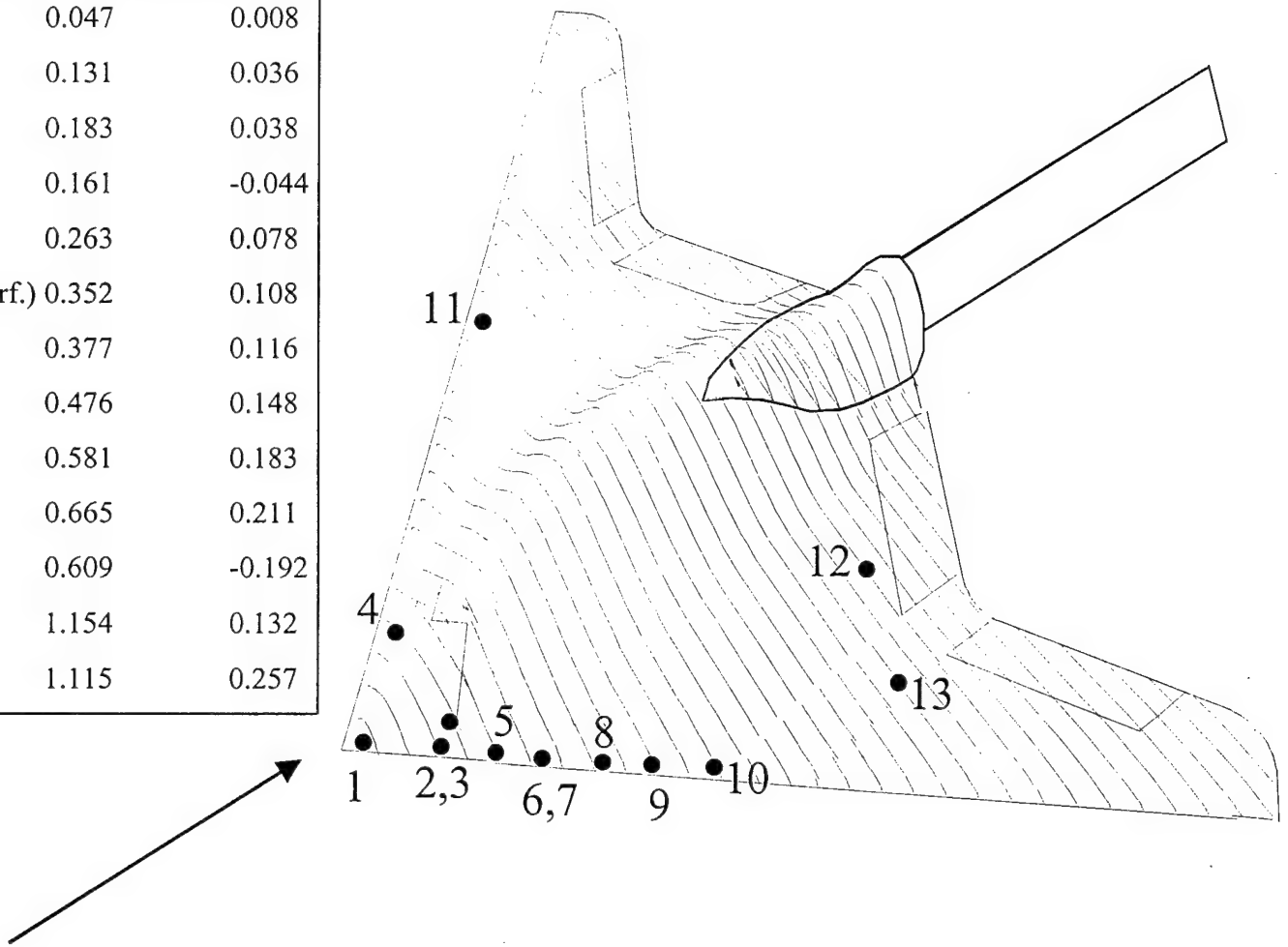

Fig. 9a- Time series data: Trans. 1

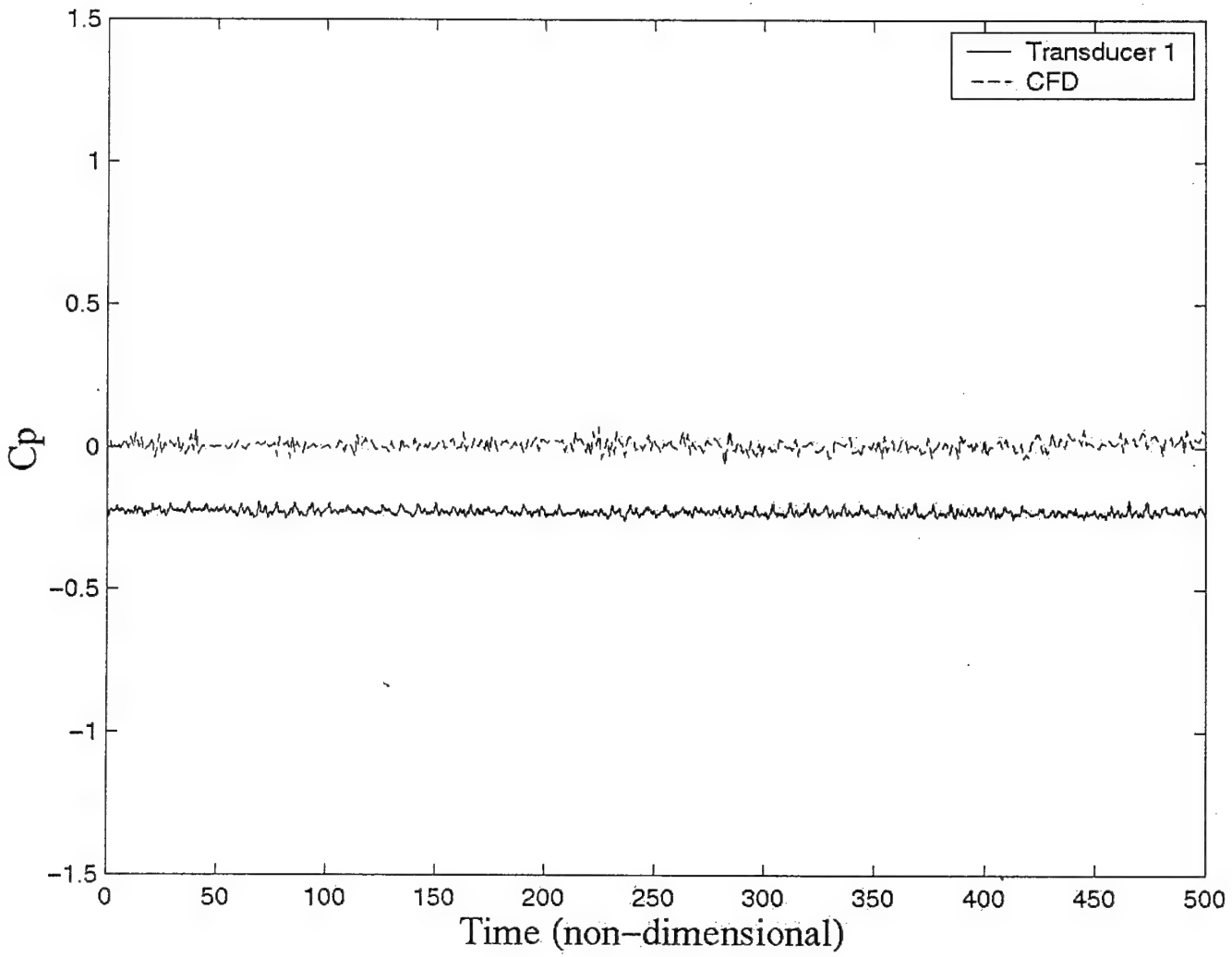

Fig. 9b- Time series data: Trans. 3

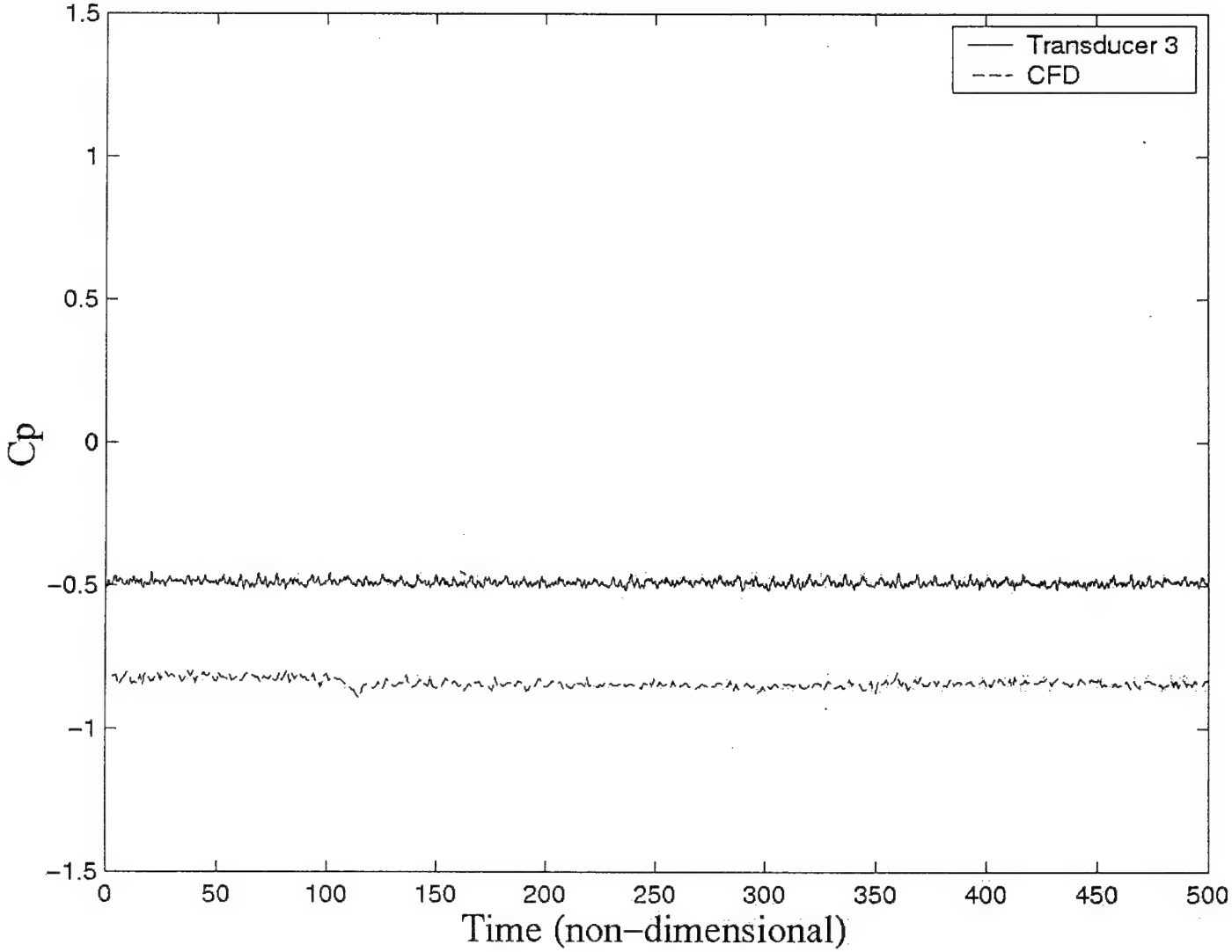

Fig. 9c- Time series data: Trans 5

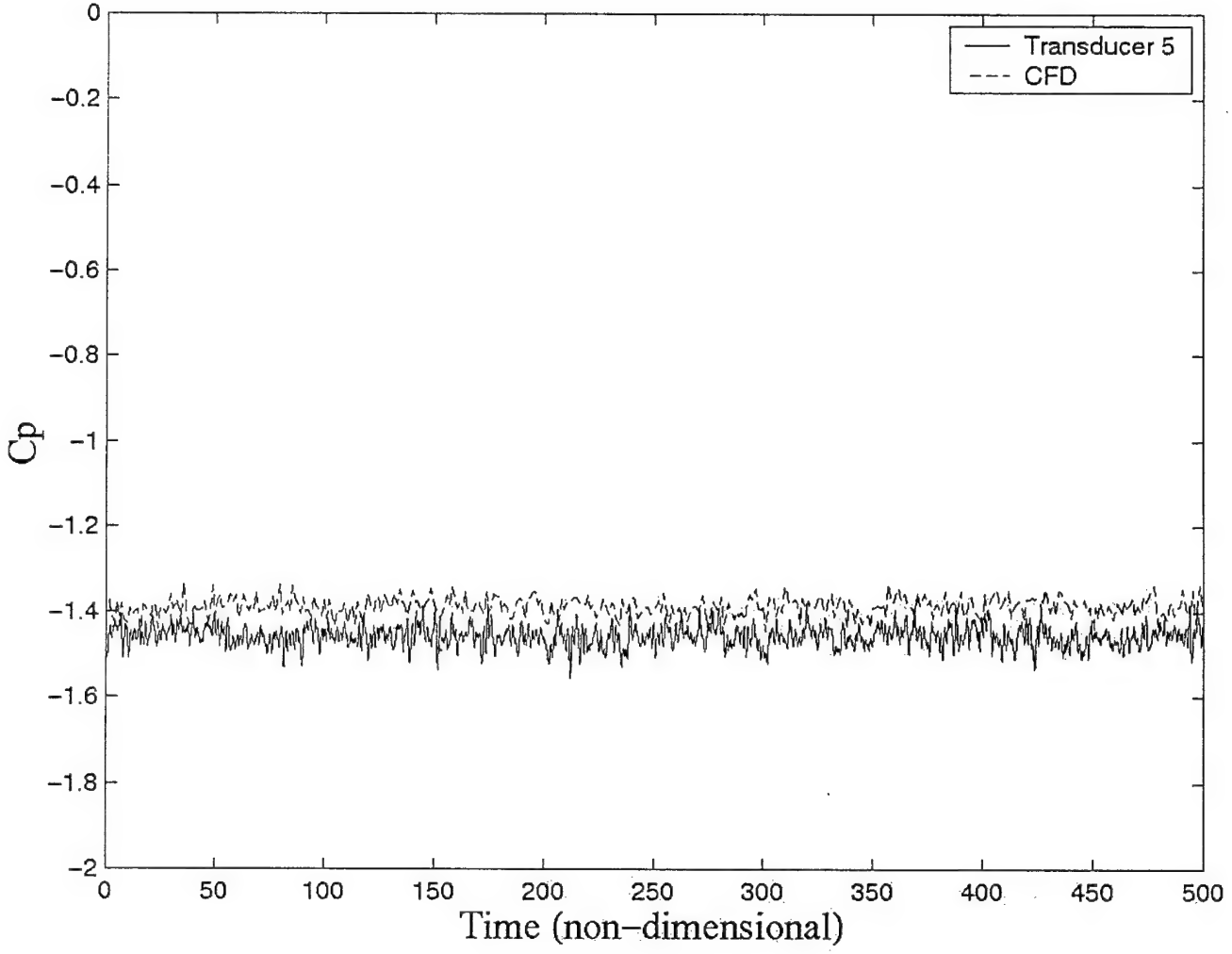

Fig. 9d- Time series data: Trans 6

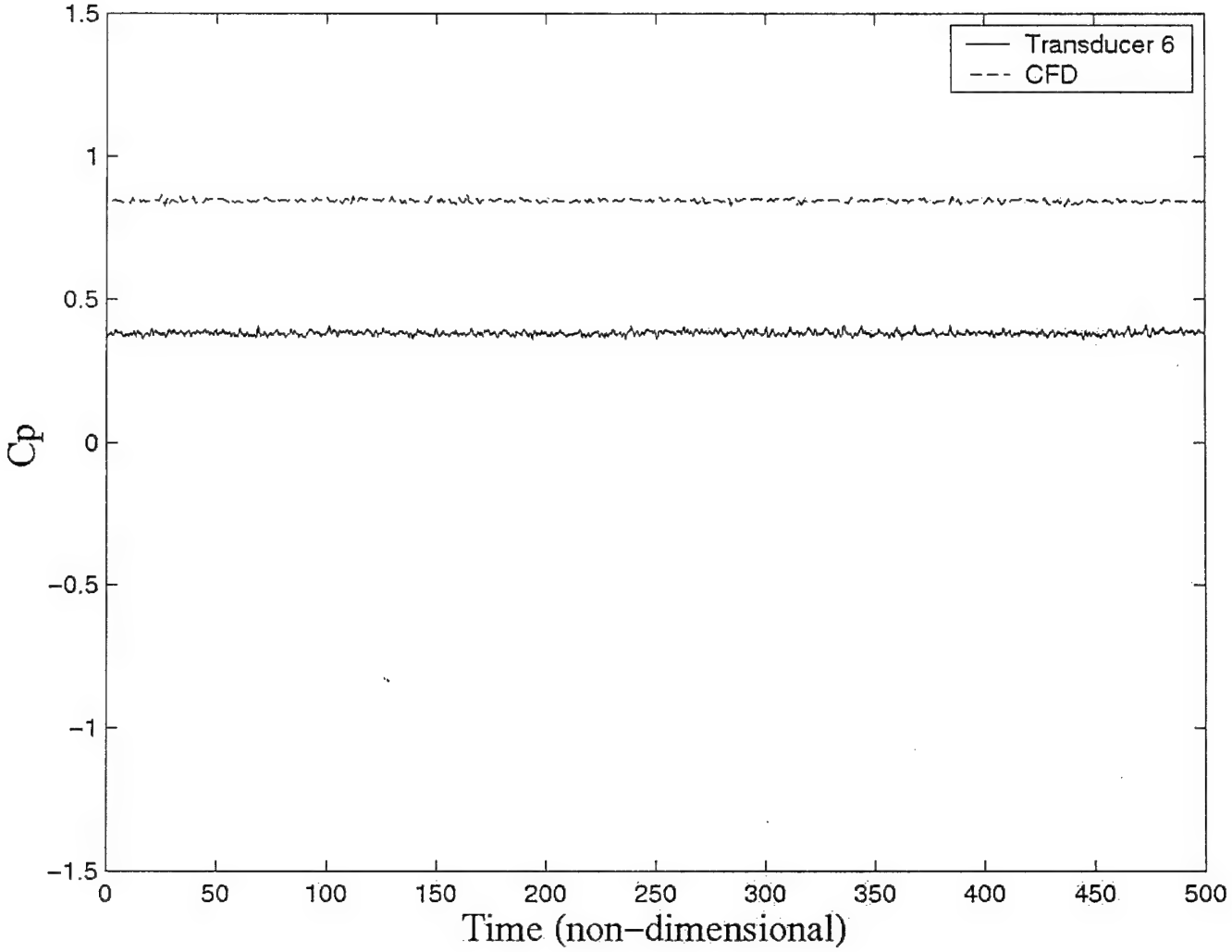

Fig. 9e- Time series data: Trans 7

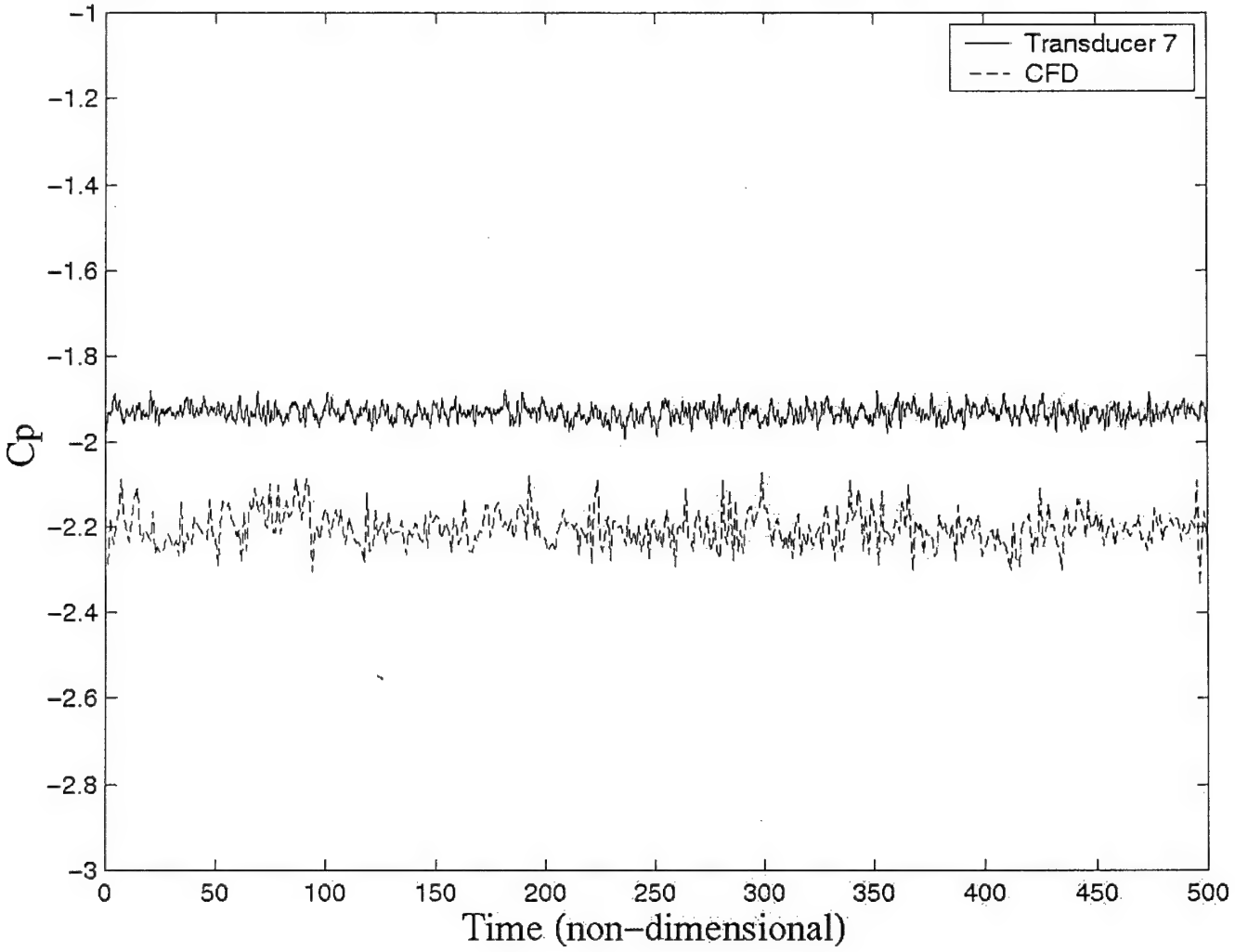

Fig. 9f- Time series data: Trans 8

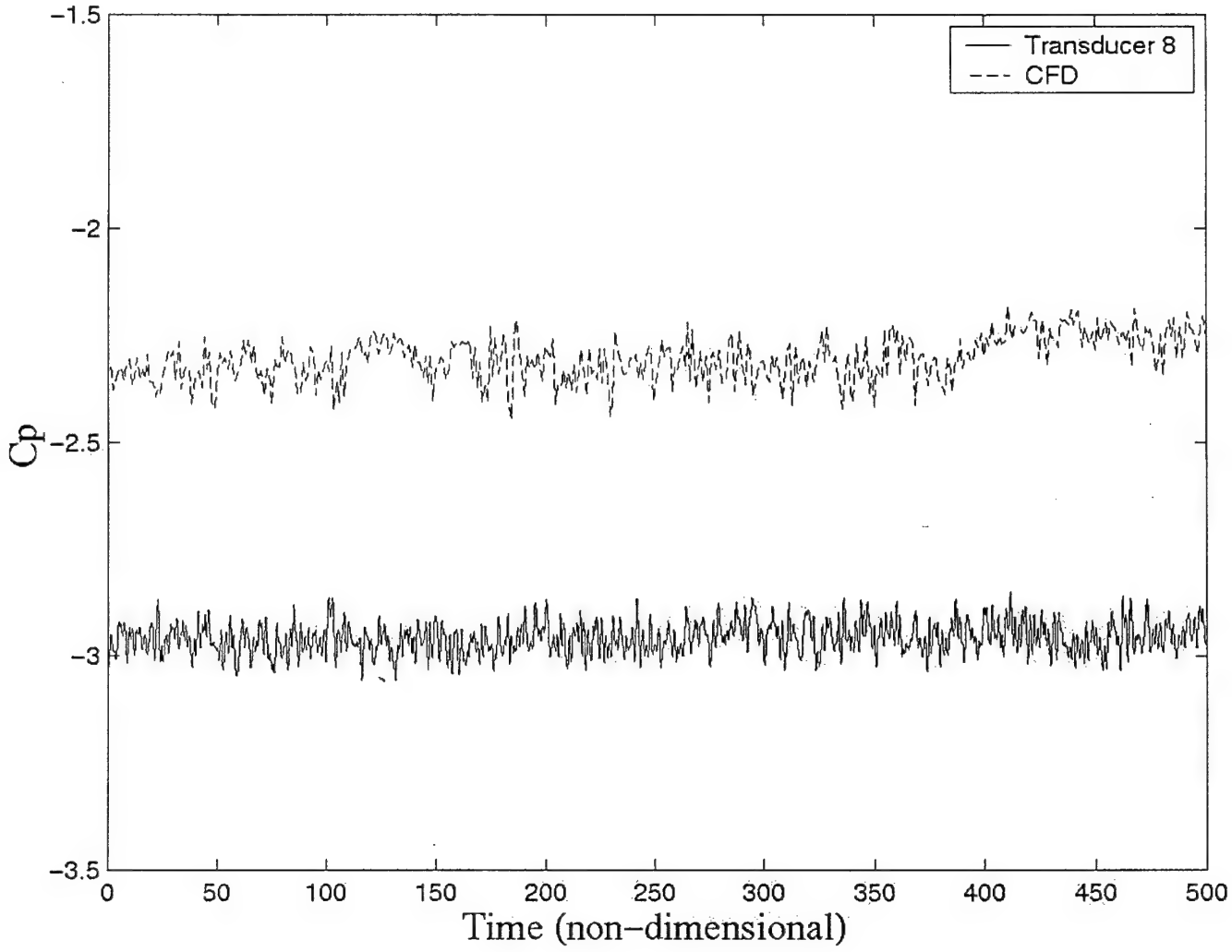

Fig. 10a- PSD data: Trans. 1

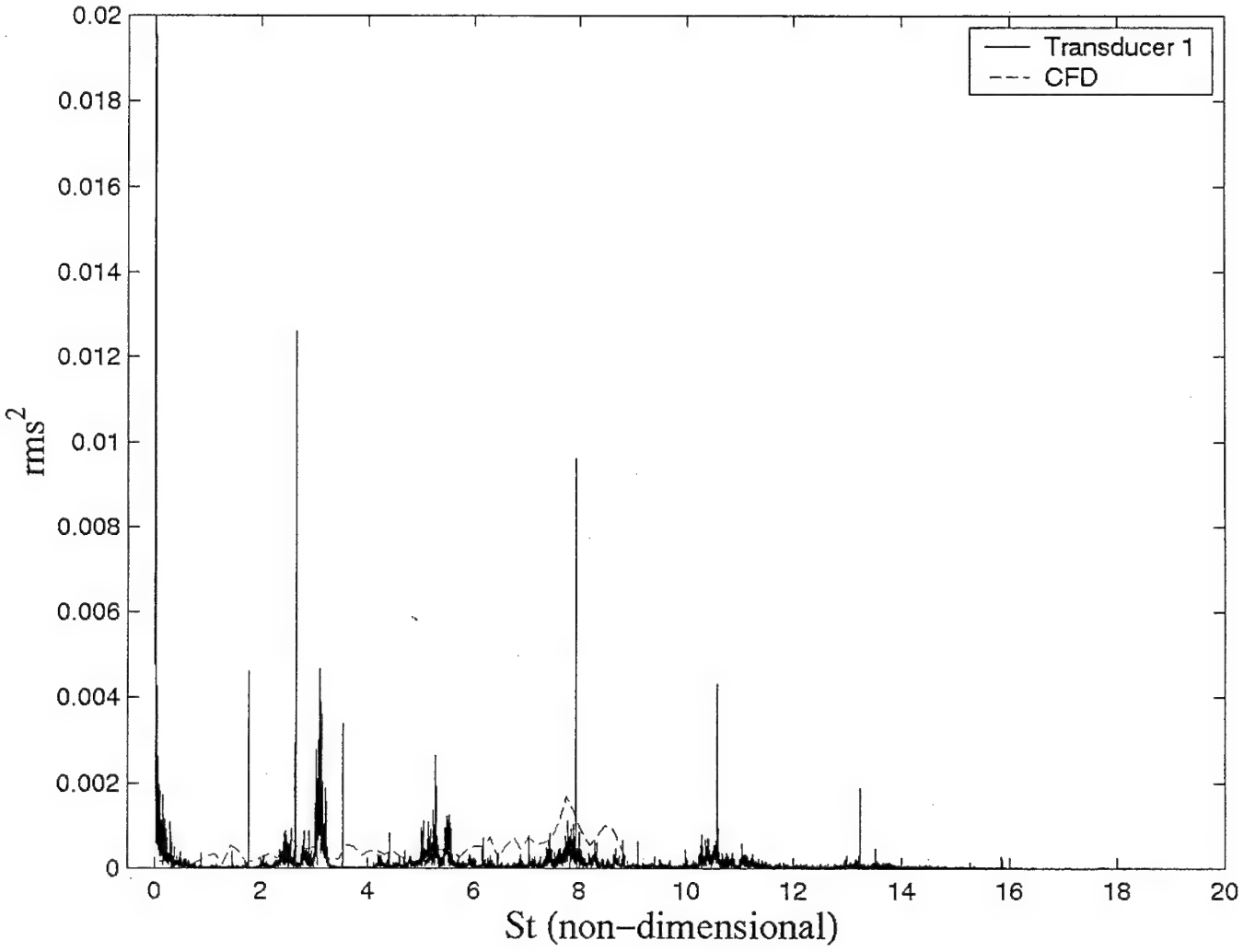

Fig. 10b- PSD data: Trans. 3

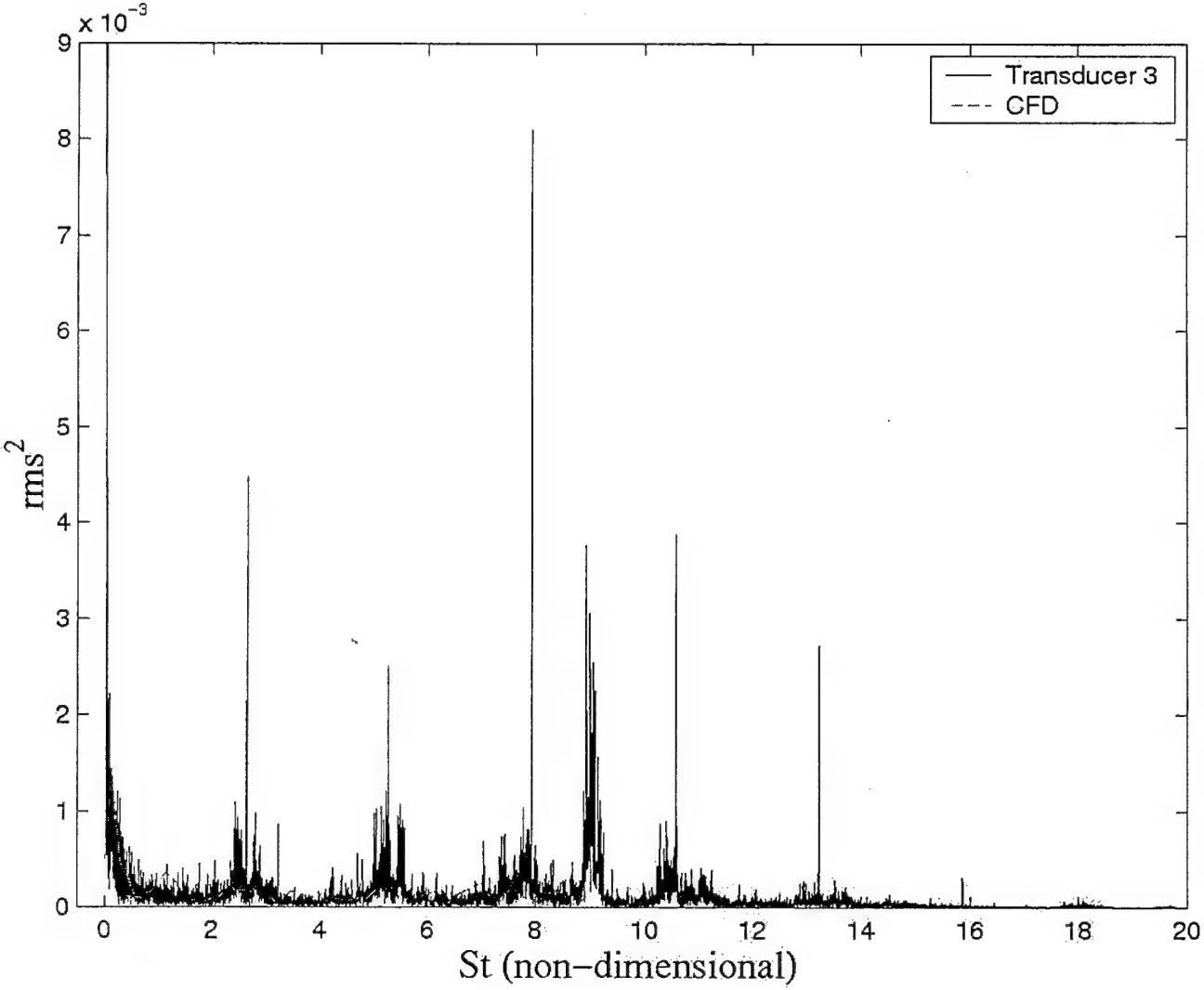

Fig. 10c- PSD data: Trans. 5

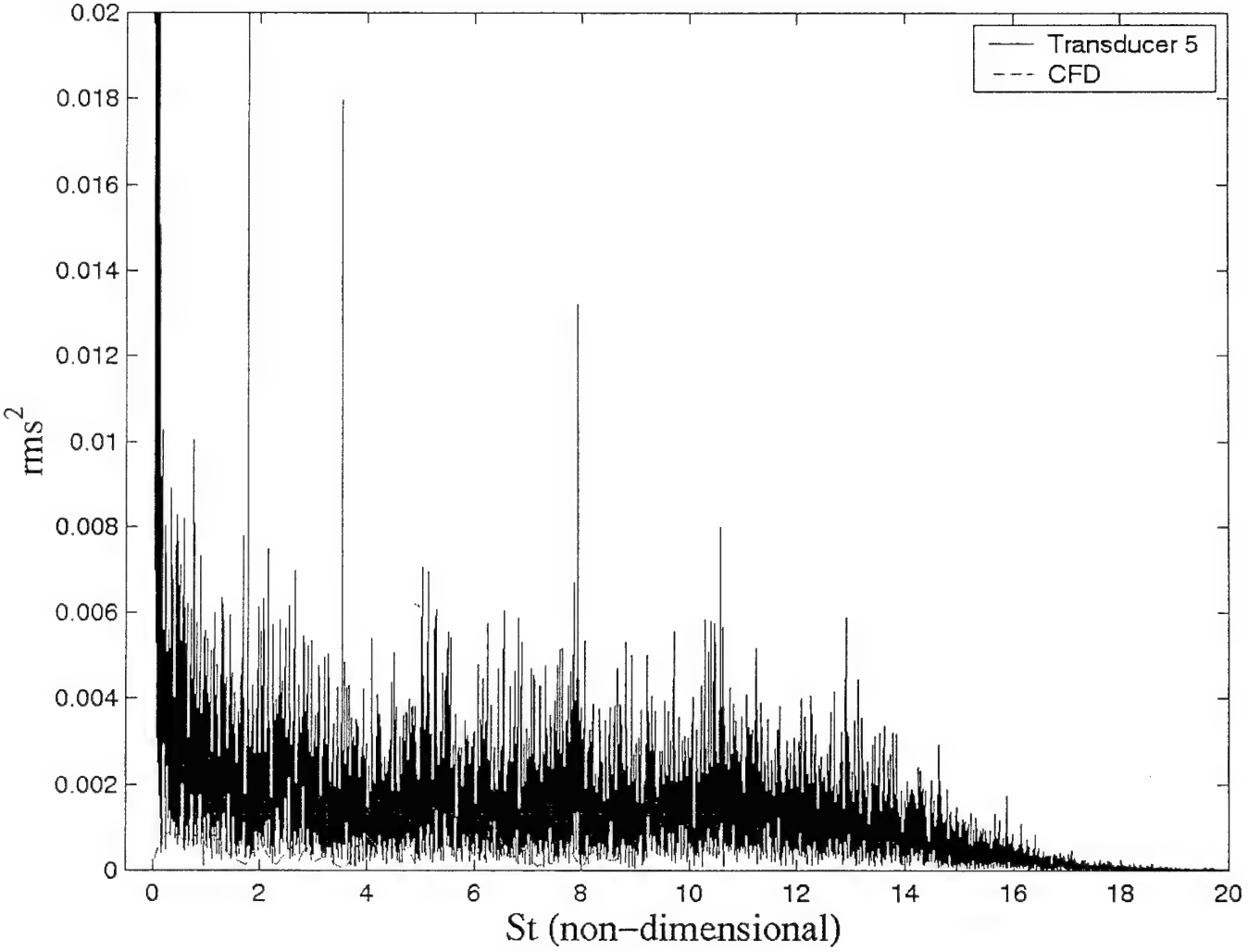

Fig. 10d- PSD data: Trans. 6

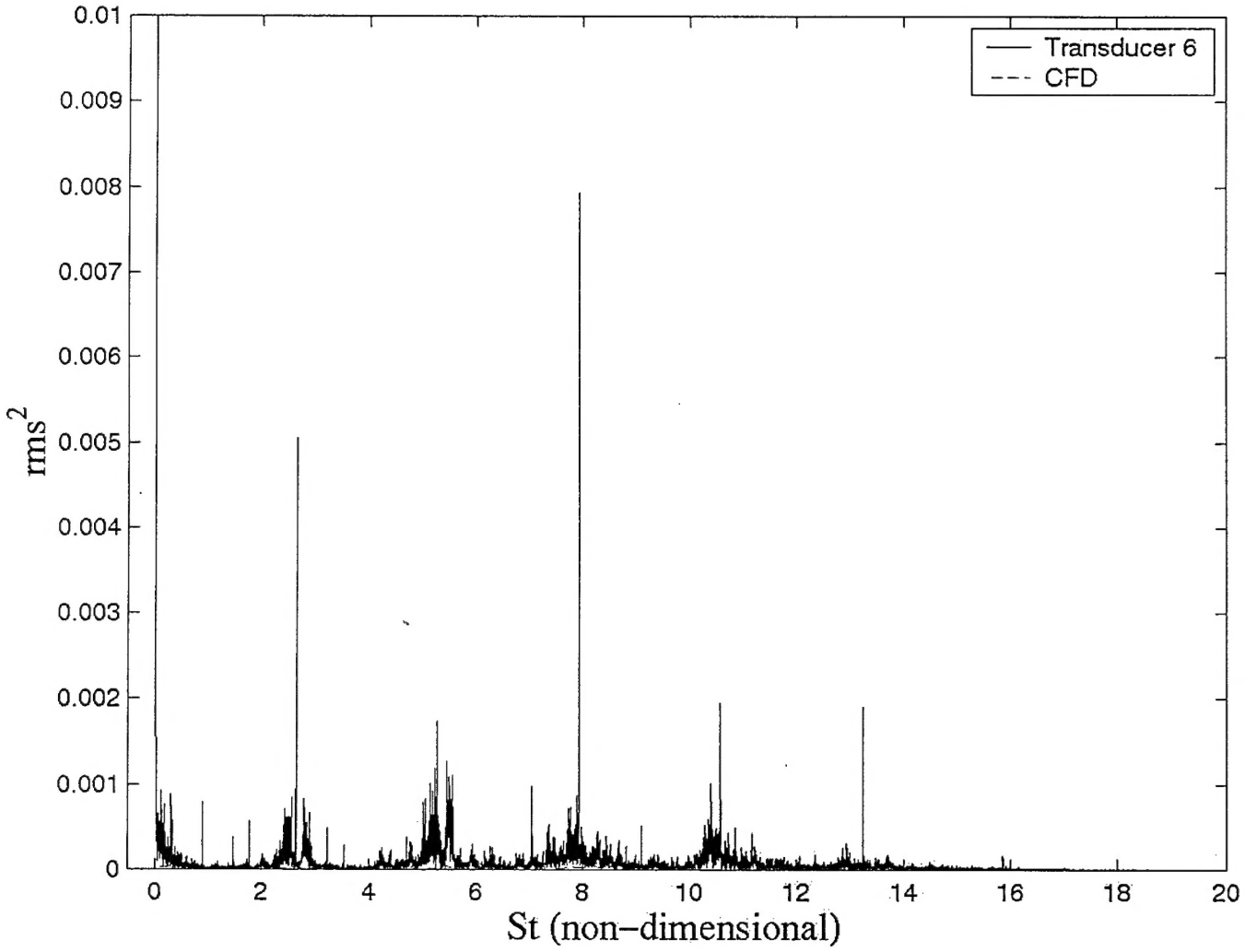

Fig. 10e- PSD data: Trans. 7

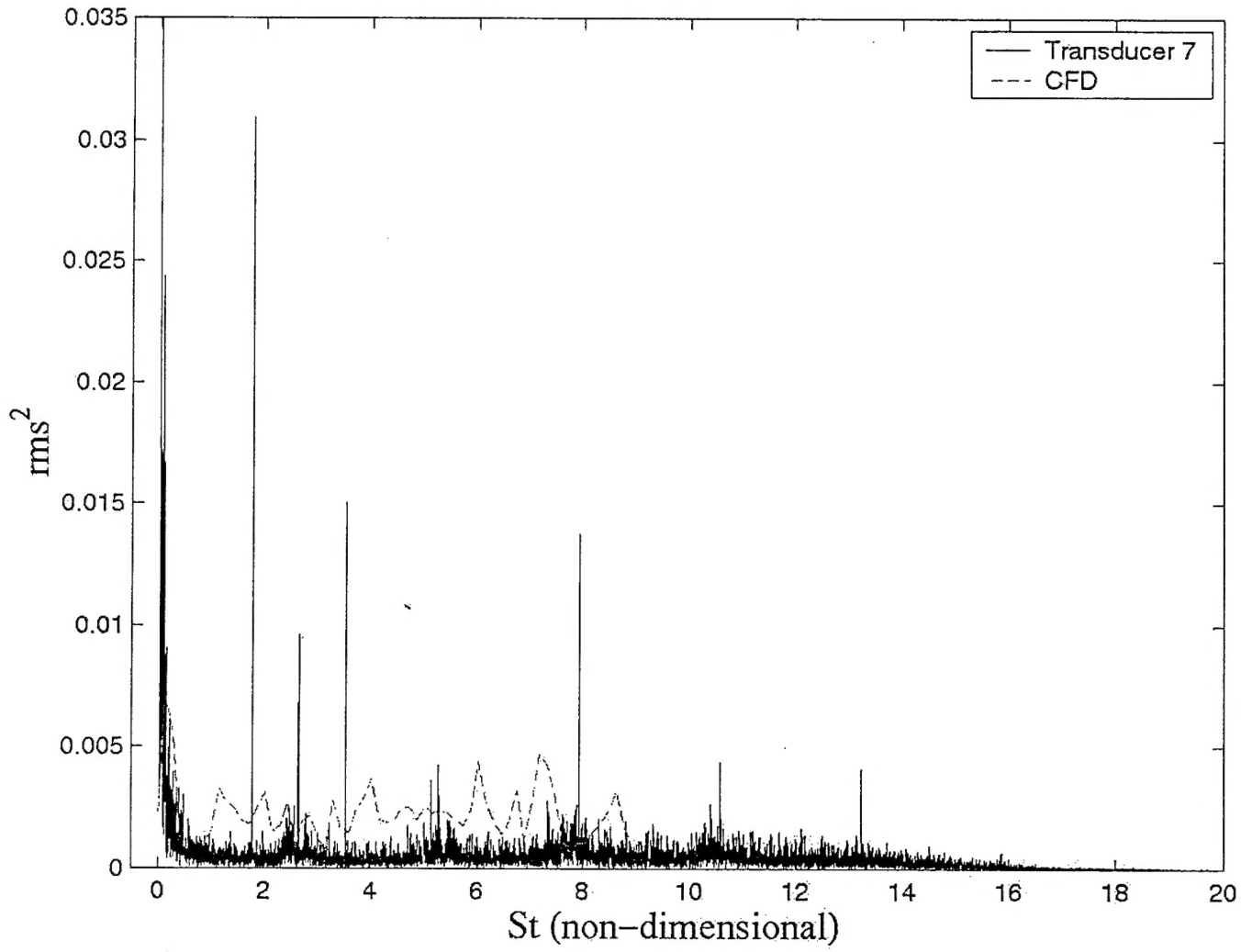

Fig. 10f- PSD data: Trans. 8

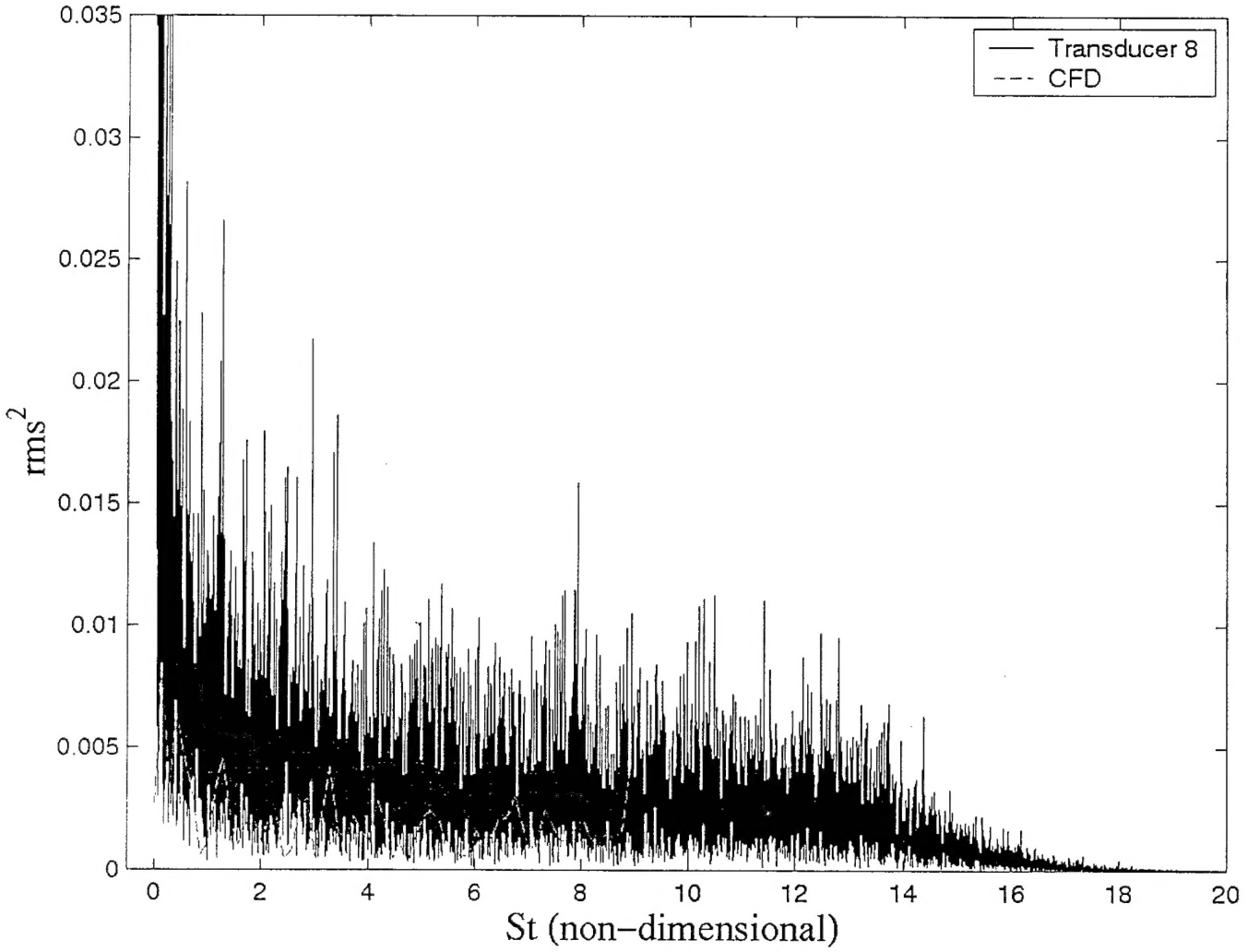

Fig. 11- Hot wire traverse system